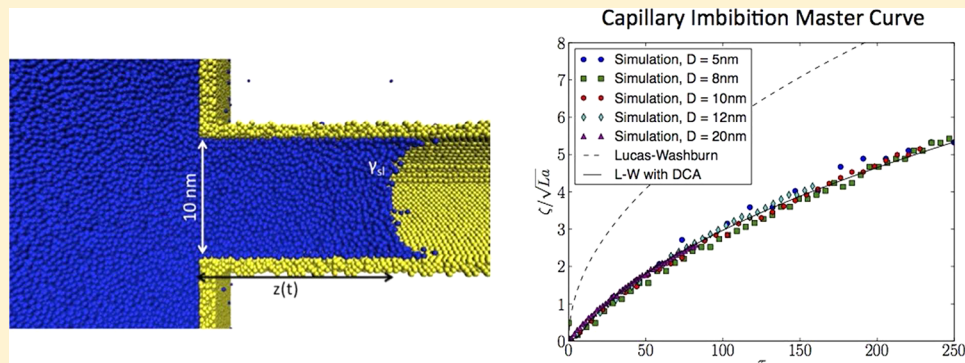


Hydrodynamics of Capillary Imbibition under Nanoconfinement

Wylie Stroberg,[§] Sinan Keten,^{*,†,‡} and Wing Kam Liu^{*,‡,||}[†]Civil and Environmental Engineering, [‡]Mechanical Engineering, and [§]Theoretical and Applied Mechanics Program, Northwestern University, 2145 Sheridan Road, Evanston, Illinois 60208, United States

Supporting Information



ABSTRACT: Understanding fluid flow in nanoconfined geometries is crucial for a broad range of scientific problems relevant to the behavior of porous materials in biology, nanotechnology, and the built environment. Because of the dominant importance of surface effects at the nanoscale, long-standing assumptions that are valid for macroscopic systems must be revisited when modeling nanoconfined fluids, because boundary conditions and the confined behavior of liquids are challenging to discern from experiments. To address this issue, here we present a novel coarse-grained model that combines parameters calibrated for water with a dissipative particle dynamics thermostat for the purpose of investigating hydrodynamics under confinement at scales exceeding current capabilities with all-atomistic simulations. Conditions pertaining to slip boundary conditions and confinement emerge naturally from particle interactions, with no need for assumptions a priori. The model is used to systematically investigate the imbibition dynamics of water into cylindrical nanopores of different diameters. Interestingly, we find that the dynamic contact angle depends on the size of the nanopore in a way that cannot be explained through a relationship between contact line velocity and dynamic contact angle, suggesting nonlocal effects of the flow field may be important. Additionally, a size-dependent characteristic time scale for imbibition is found, which could be useful for the interpretation of experiments and design of novel nanofluidic devices. We present the first systematic study that explains how contact angle dynamics and imbibition dynamics vary with nanopore radius. Our modeling approach lays the foundation for broader investigations on the dynamics of fluids in nanoporous materials in conjunction with experimental efforts.

INTRODUCTION

The behavior of fluids in confined nanoscale geometries is strongly influenced by surface effects and interfacial dynamics, presenting fundamental challenges to the application of long-standing macroscopic theories of flow and mass transport phenomena to these systems. Computational methods provide a very reliable methodology for accurately quantifying the factors governing transport under these conditions. For very small systems, such as flow through carbon nanotubes, molecular dynamics simulations have proven useful to resolve single-file flow mechanisms.^{1,2} At length scales on the order of micrometers, continuum models provide accurate predictions in conjunction with experiments. However, many systems of interest lie in a mesoscopic scale that emerges in the submicrometer to a few nanometers range. At these length scales, system sizes are often too large to be modeled with all-atom models, yet continuum descriptions require prescription of key physics such as boundary slip conditions. Capillary forces

and related imbibition processes that occur in these systems are critical for a range of applications. For example, nanopores in lab-on-a-chip devices selectively transport biomolecules for detection, diagnostics, and separation applications. Dry nanoporous silica microparticles loaded with active nanoparticle solutions through capillary imbibition have recently been developed for improving efficacy in precise drug delivery and medical imaging applications.³ Nanopatterned surfaces in electronics and multifunctional materials exhibit novel adhesion, adsorption, and wetting phenomena that are also strongly influenced by nanopore bridges that form between two nanoscopic contact surfaces.⁴ In nanoscale thin films and surfaces employing nanopillars, collapse of nanostructural patterns due to capillary action has been observed, in both

Received: June 6, 2012

Revised: August 27, 2012

Published: August 29, 2012

dysfunctional and functional contexts.^{5,6} Understanding novel physical phenomena that emerge in the nanoscale confined interfaces between liquids and solids is foundational for exploiting new functionalities obtained by nanostructuring and for overcoming numerous obstacles in the way of technological advances that rely on extreme miniaturization.

In experiments as well as all-atom models, these boundary conditions emerge naturally from the discrete molecular nature of the fluid and solid interfaces and flow conditions.⁷ For mesoscopic systems in confined geometries, interface conditions can significantly contribute to the system's dynamics, and inaccurate prescription of these boundary conditions can lead to significant errors in continuum models. Therefore, new computational techniques are needed to understand dynamics of fluids under nanoconfinement that are capable of retaining the emergent properties of atomistic simulations, while reaching length and time scales outside the current capabilities of all-atom molecular dynamics. For systems in equilibrium, such as simulations of biomolecules, where water acts as a solvent, coarse-grained molecular dynamics (CGMD) models have been shown to accurately reproduce the results of classical molecular dynamics (MD), while greatly reducing computational cost.^{8,9} However, for many transport problems, the judicious choice of potential parameters does not suffice to capture hydrodynamic details. In particular, for out-of-equilibrium conditions such as capillary imbibition and drainage, global thermostats like the Nose–Hoover, which dissipates energy globally by coupling the system to an additional degree of freedom, require a sufficiently large number of particles to correctly reproduce hydrodynamics.¹⁰ Furthermore, in cases where there exists a net flow field in the fluid (e.g., capillary imbibition, Couette flow), it is necessary to thermostat the system without biasing the flow toward a certain reference frame. Local thermostats that rescale particle velocities relative to a viscous background (e.g., Brownian dynamics, Langevin thermostats) fail to preserve momentum by biasing the particle motion toward a “laboratory” or stationary reference frame and thus cannot capture hydrodynamics accurately. A popular solution to these issues is to use a dissipative particle dynamics (DPD) thermostat.¹¹ In a DPD thermostat, particle velocities are rescaled through pairwise interactions with neighboring particles in such a way that the system both satisfies the fluctuation–dissipation theorem and preserves momentum. Although classically coupled with a purely repulsive conservative force, it is possible to combine a DPD thermostat with any conservative force field, making it ideal for modeling a wide range of fluid transport problems. The most prevalent fluid transport problems are those involving water; however, to date, DPD has not been coupled to a conservative potential to realistically simulate dynamic behavior of water at the mesoscale.

To address this issue and thereby provide a reliable method for studying mesoscale hydrodynamics of water, here we present a calibrated water model combined with a DPD thermostat that can be applied to study a broad range of fluid transport problems. Our hybrid modeling approach combines the desirable aspects of the force field-based MD methodology with DPD thermostatting procedure to accurately capture the surface tension, density, and viscosity of water. Furthermore, we present large-scale massively parallel simulations of imbibition of water into a nanopore, to confirm the ability of this model to simulate mesoscale hydrodynamics problems. Finally, we compare our simulations with theoretical models and show

that simulation results for a broad range of nanotube sizes can be predicted by a modified, nondimensionalized Lucas–Washburn equation that considers contact angle dynamics.

METHODOLOGY

Historically, the aim of DPD was to make fluid dynamic behavior correctly emerge from a particle-based simulation method,¹² while using the simplest interactions possible. In its traditional form,^{11,13,14} the interparticle force for each particle is given by

$$\mathbf{f}_{ij} = (F_C + F_D + F_R)\hat{r}_{ij} \quad (1)$$

where F_C , F_D , and F_R are magnitudes of a conservative force, a dissipative force, and a random force, respectively, and \hat{r}_{ij} is a unit vector along the line connecting particle i to particle j . The classical DPD conservative force is given by

$$F_C = Aw(r) \quad (2)$$

where A is a constant and w is a weight function defined, for simplicity, as $w = 1 - r/r_c$ for $r < r_c$ and $w = 0$ for $r > r_c$. The dissipative force acts as an equal and opposite drag force on pairs of particles and is given by

$$F_D = -\xi w^2(r)(\hat{r}_{ij} \cdot \mathbf{v}_{ij}) \quad (3)$$

where ξ modulates the strength of the dissipation, and $\hat{r}_{ij} \cdot \mathbf{v}_{ij}$ gives the velocity along the line connecting the particle centers. The random force to offset the energy lost through dissipation is determined by the fluctuation–dissipation theorem to be

$$F_R = \sigma w(r)\alpha\Delta t^{-1/2} \quad (4)$$

where $\sigma = (2k_B T\xi)^{1/2}$, and α is a Gaussian random number with mean zero and variance one.

However, with this form, liquid–vapor interfaces cannot be modeled because the purely repulsive conservative force causes the particles to completely fill the simulation box. In addition, the transferability of the model to modeling mechanics problems such as those related to polymer–solvent mixtures remains limited, because the softer potentials allow molecular overlap. Several modifications to the conservative potential have been made to model interfaces. Pagonabarraga and Frenkel¹⁵ and Warren¹⁶ have presented conservative forces based on local weighted densities, which allows for equations of state containing van der Waals loops, and hence liquid–vapor coexistence. These methods inherently require many-body potentials, which come at a higher computational cost and are more difficult to integrate into standard, parallelized MD codes. Soddemann et al.¹⁰ have emphasized the utility of viewing DPD as a thermostat that can be used with any interatomic potential. Along these lines, several studies of capillarity and wetting have been conducted using Lennard–Jones (LJ) potentials.^{17,18} These studies have been useful in qualitatively investigating the dynamics of fluids at the mesoscale, but in many cases it is desirable to be able to quantitatively predict how a specific fluid (often water) will behave. Predictive capabilities require a well-calibrated model for the interparticle potential. For water, several coarse-grained models have been developed for use as an explicit solvent during biomolecular simulations. Most popular among these is the MARTINI model,¹⁹ which relies on a LJ potential. The model has been largely successful as a solvent, but has several troubling features including crystallization near interfaces at room temperature, making it less than ideal for simulations in confined geometries such as capillaries. Chiu et al.⁹ have suggested a water model based on a softer, Morse potential that does not readily form lattice structures near surfaces, and thus is much better suited for simulations of nanoconfined systems. Although the softer potential does lead to a self-diffusion coefficient roughly twice the experimental value, the model's careful calibration of density and surface tension, as well as its ability to model confined fluids, more than makes up for this discrepancy. Furthermore, as pointed out in ref 9, the diffusion coefficient of a coarse-grained model may not be the most relevant metric, because experimental observations are based on the movement of single water molecules, which do not exist in coarse-grained models.

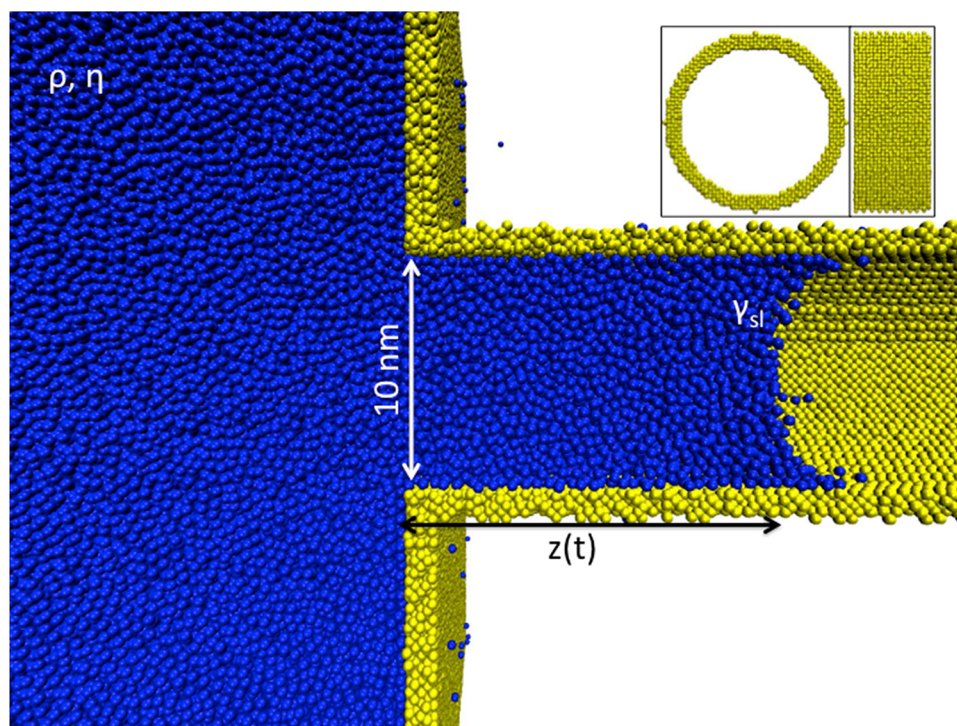


Figure 1. Snapshot of imbibition simulation at 3.7 ns. Initially, the nanopore is sealed while the fluid equilibrates, then the cap is removed and the fluid fills the nanopore. Capillaries with diameters of 5, 8, 10, 12, and 20 nm were simulated. System is periodic in x - and y -directions. Fluid properties such as surface tension, density, and viscosity are calibrated to match the properties of bulk water. The roughness on the exterior of the pore is largely due to the perspective view of the snapshot. The inset cross-sectional slice provides a more accurate rendering of the pore roughness.

The model constructed by Chui et al. was designed for CGMD simulations at equilibrium so fluid viscosity was not considered during the calibration. In nonequilibrium hydrodynamics simulations, such as wetting, fluid viscosity plays an important role; thus the conservative force for the model presented here is derived from a Morse potential, calibrated to match not only the density and liquid–vapor interfacial tension but also the viscosity of water.

As a demonstration of the model's capability of capturing mesoscale hydrodynamic phenomena, fluid imbibition into nanopores of varying diameter was simulated. The system (Figure 1) consisted of a cylindrical nanopore 50 nm in length in contact with a 50 nm \times 10 nm \times 10 nm reservoir of fluid. Model pores with diameters ranging from 5 to 20 nm were tested. The reservoir dimensions were large enough as compared to the nanopore diameter such that periodic boundary conditions could be used without any significant influence from neighboring pores on the filling dynamics. The nanopore walls consisted of an fcc lattice of particles tethered to their initial position by linear springs with spring constant $k = (k_B T)/(a^2)$, where k_B is Boltzmann's constant and a is the fcc lattice constant, which has a value of 0.5 nm. The wall thickness in all simulations is 1.0 nm. The nanopore is not intended to model any particular material, but instead provides a general model in which the degree of hydrophobicity of the surface can be readily adjusted. The particle–wall interactions are modeled using a Morse potential with parameters chosen to attain no-slip fully wetting boundary conditions characteristic of hydrophilic surfaces. The equilibrium contact angle between the water and the nanopore surface was determined to be 0° in separate contact angle simulations (see Figure S2 in the Supporting Information). Initially, the nanopore inlet was sealed and the reservoir was allowed to equilibrate for 1 ns, long enough for sizable temperature and pressure fluctuations to decay. After equilibration, the inlet was opened and the fluid was drawn into the nanopore through capillary suction. Dynamic contact angles were obtained directly from simulations in a method similar to that in refs 20–22 with the exception that the menisci were fit using parabolic as opposed to circular functions. In all cases, particles within 0.629 nm of the wall were omitted from the fitting to

avoid regions that substantially deviate from the mean curvature of the meniscus. We find that contact angles calculated from parabolic fits match those from circular fits to within a few degrees. For the smallest nanopore studied (5 nm diameter), over one-half of the cross-sectional area lies within the region that deviates from hemispherical due to interactions with the wall, implying a circular fit may not capture the meniscus curvature well in this case. The circular fits are also more sensitive to the thickness of the excluded region than are parabolic fits. For these reasons, we believe parabolic fits offer a more consistent means of calculating contact angles across the pore sizes studied in this work. In all imbibition simulations, a time step of 20 fs was used with an NVE integrator and DPD thermostat. The cutoff length for the potential was set to 1.6 nm following ref 9.

All simulations were carried out using LAMMPS software.²³ Trajectories were visualized with VMD.²⁴

RESULTS AND DISCUSSION

As a starting point for our model, we directly implemented the Morse potential reported in ref 9 in our model and verified that the density and surface tension values are in reasonable agreement with that of water. The Morse potential used in our model has the form:

$$U_{ij} = \epsilon [e^{-2\alpha(r-R_0)} - 2e^{-\alpha(r-R_0)}], \quad r < r_C \quad (5)$$

where ϵ represents the potential well depth, α controls the width of the depth and thus the stiffness of the interaction, and R_0 is the equilibrium distance between particles. r_C is the cutoff distance for the conservative force field and was set to be 1.6 nm following ref 9. The analytical form of the equation used here is slightly different from that used in ref 9 (due to the implementation used in LAMMPS), but the two potentials are easily shown to be equivalent and the parameters are readily convertible from one form to another. Therefore, the corresponding parameter values for the form of the potential

used here are: $\epsilon = 0.813$ kcal/mol, $\alpha = 0.556 \text{ \AA}^{-1}$, and $R_O = 6.29 \text{ \AA}$.

Viscosity plays an essential role in hydrodynamics problems and, in DPD, results from the summation of a kinetic and a dissipative component. The kinetic contribution decreases with increasing damping parameter, ξ , while the dissipative portion increases linearly with ξ .²⁵ Hence, for large values of the damping parameter, the dissipative contribution dominates, and the viscosity can be controlled by ξ . To calibrate the damping parameter to match the viscosity of water, Couette flow was induced in a rectangular fluid box between two solid plates. The top plate was sheared at a constant rate, which led to a linear velocity profile being created in the fluid. The components of the pressure tensor parallel to the velocity could then be averaged over the ensemble to give an estimate of the shear stress in the fluid. By shearing the top plate at different rates, a linear relationship was obtained between the shear rate and the shear stress, the slope of which gives the fluid viscosity (shown in Figure S1 in the Supporting Information). Using this technique, a viscosity of $(9.0 \pm 0.01) \times 10^{-4} \text{ Pa}\cdot\text{s}$ was obtained for $\xi = 2850 \text{ kcal}\cdot\text{fs}/\text{mol}\cdot\text{A}^2$. Strictly speaking, the viscosity of a DPD fluid will also depend on the time step,²⁶ so all simulations, including those used to calibrate the viscosity, have been performed consistently with a time step of 20 fs.

Following the viscosity calibration, the surface tension and density of the model were measured to ensure that the values were in reasonable agreement with that of bulk water. To do this, a periodic simulation box was half-filled with particles and allowed to equilibrate, forming a slab of water with two free surfaces. Following ref 27, the surface tension was estimated using the anisotropy of the pressure tensor:

$$\gamma = \frac{L_z}{2} \left[\langle P_{zz} \rangle - \frac{1}{2} (\langle P_{xx} \rangle + \langle P_{yy} \rangle) \right] \quad (6)$$

where z corresponds to the coordinate normal to the slab. Using this technique, the surface tension was found to be $0.070 \pm 0.005 \text{ N/m}$, which compares reasonably well with experimental values for water at room temperature (0.072 N/m). To measure the density of the fluid, a separate NPT simulation with a periodic box of 24 000 coarse-grained beads was simulated for 5 ns at 298 K. The density was found to be $0.999 \pm 0.001 \text{ g/cm}^3$, as compared to experimental values for room temperature water (0.998 g/cm^3). These values show good agreement with those found in ref 9 (density of 0.998 g/cm^3 , surface tension of 0.071 N/m). Thus, the present model still well represents the properties of water with the added benefit of a finely tuned viscosity, making this model useful for dynamic simulations of water.

To demonstrate the capability of the model in capturing mesoscale hydrodynamic phenomena, we simulated the spontaneous imbibition of water into nanopores due to the capillary effect. Here, we present results from these imbibition simulations, where we investigated the imbibition rates for hydrophilic (fully wetting) nanopores ranging in diameter from 5 to 20 nm. The parameters for the Morse potential governing the interaction between fluid and nanopore particles are: $\epsilon = 0.8$ kcal/mol, $\alpha = 0.55 \text{ \AA}^{-1}$, and $R_O = 4.9 \text{ \AA}$. Figure 2 shows the results of imbibition simulations for different nanopore diameters. The initial stages of the imbibition process are very similar, which suggests that the fluid travels approximately the same distance in each pore as a function of time in the early stages of the imbibition process. However, after a few nanoseconds, the curves for different diameter channels begin

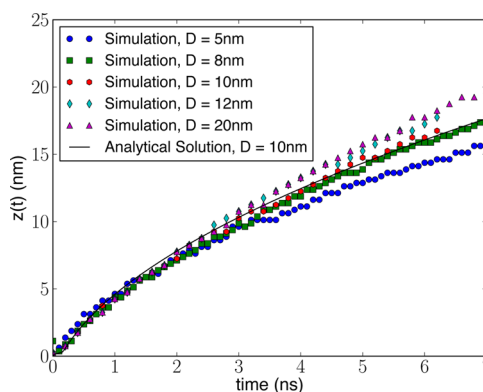


Figure 2. Nanopore imbibition length as a function of time for different diameter capillaries. The dynamics of the capillaries begins to diverge around 2 ns, with larger capillaries filling more rapidly.

to diverge, and a clear trend emerges. In particular, we observe that the smaller channels tend to fill more slowly than the larger ones. An understanding of these results and, more generally, nanoscale capillary imbibition can be formed by comparison to theoretical solutions for larger pores.

At the microscale, capillary imbibition can be accurately described through the Lucas–Washburn (LW) equation:^{28,29}

$$z(t) = \sqrt{\frac{\gamma R_v \cos \theta_E}{2\eta} t} \quad (7)$$

where z is the imbibition length, γ is surface tension, R_v is the volumetric pore radius, θ_E is the equilibrium contact angle, and η is the fluid viscosity. However, applicability of this equation to nanoscale systems has remained a subject of much controversy, where several studies employed computational methods such as large-scale molecular dynamics to explain what amendments need to be considered when the LW equation is employed to quantify flow in channels with small dimensions (sub 100 nm). Martic et al.^{18,22} simulated the imbibition of a Lennard-Jones fluid into a nanopore and found that when the energy dissipation at the contact line is large as compared to the viscous dissipation in the bulk fluid, as is often the case with nanoscale capillaries, the LW equation fails to accurately describe the penetration. In such cases, the LW equation must be modified to account for a DCA. This result has been confirmed by a number of other studies using DPD.^{18,20,21,30} The derivation of the LW equation also neglects inertial effects. However, in the early stages of imbibition, the inertia prevails over viscosity. The time scale where inertia is significant and the system is in the Bosanquet regime³¹ is given dimensionally as $t_v = (\rho R_v^2)/(\eta)$. For water in a 10 nm radius channel, $t_v \approx 0.1 \text{ ns}$, implying the inertial effects are negligible for all but the very earliest times and likely have little influence over the long-time scale imbibition dynamics. Thus, accounting for the DCA and neglecting inertial effects, the equation of motion governing the imbibition dynamics can be written as:

$$0 = F_{\text{cap}} - F_{\text{visc}} = 2\pi R_v \gamma \cos \theta_D - 8\pi \eta z z' \left(\frac{R_v^2}{R_d^2} \right) \quad (8)$$

where F_{visc} is the resistive force due to wall friction, and θ_D is the dynamic contact angle (DCA). Following ref 30, R_v is the volumetric or static radius, and R_d is the hydrodynamic radius, which depends on the roughness and wettability of the surface. In an ideally smooth surface with no surface slip, $R_d = R_v$.

However, for atomically rough nanopores with strong fluid–surface interactions, as is the case in the present simulations, R_d can be significantly smaller than the volumetric radius.³⁰ Rearranging terms and integrating eq 8 with respect to time, we obtain a modified Lucas–Washburn equation with the form:

$$z(t)^2 = \frac{R_{\text{eff}}\gamma}{2\eta} I \quad (9)$$

where $R_{\text{eff}} = (R_d^2)/R_v$ is an effective radius, and $I = \int_0^t \cos \theta_D(\hat{t}) d\hat{t}$ is the time integral of the DCA. It is challenging to obtain the hydrodynamic radius exactly from simulations or experiments. One might expect that it would take the form $R_d = R_v - c$, where c is a constant that depends only on the roughness and interaction between the wall and fluid. However, from the simulations of different size nanopores (Figures 2–

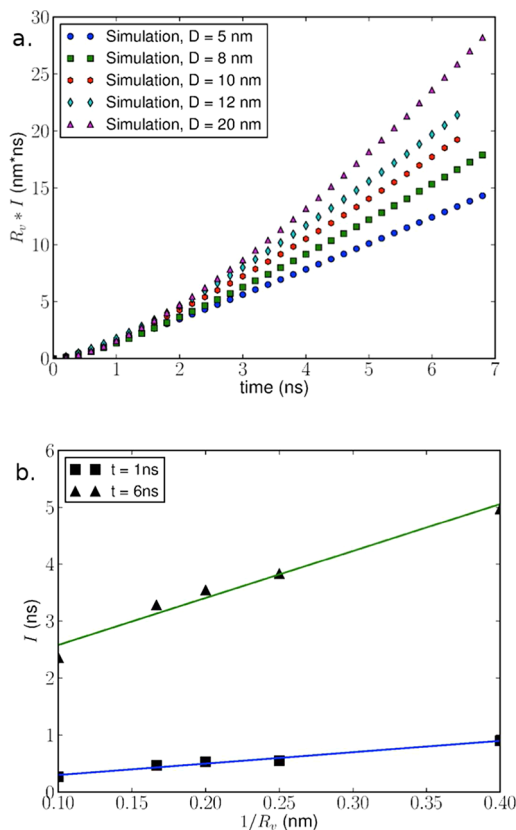


Figure 3. (a) The time-integral of the cosine of the dynamic contact angle times the nanopore radius as a function of time. Initially, the plots overlap, suggesting that the right-hand side of eq 8 should be independent of nanopore size at small times. After a few nanoseconds, the curves diverge, causing the imbibition dynamics (eq 9) to show a significant dependence on the nanopore size. (b) Integral of the dynamic contact angle, I , as a function of inverse radius at time = 1.4 and 6 ns. The solid lines represent linear fits, with normed residuals of 0.010 and 0.027 for $t = 1.4$ and 6 ns, respectively, showing the divergence from a $1/R_v$ relationship as time increases.

4), we find that the hydrodynamic radius variation cannot be adequately represented by an equation of this form. Instead, all pore sizes are captured by a model that assumes R_d scales linearly with the volumetric radius, allowing R_{eff} to be equivalent to $C_d R_v$, where $C_d = R_d^2/R_v^2$ is a numerical coefficient that is taken as a constant over the range of radii included in this study. From the simulations, we find that $R_d = 0.61R_v$, which corresponds to $C_d = 0.37$. Introducing this constant is, in

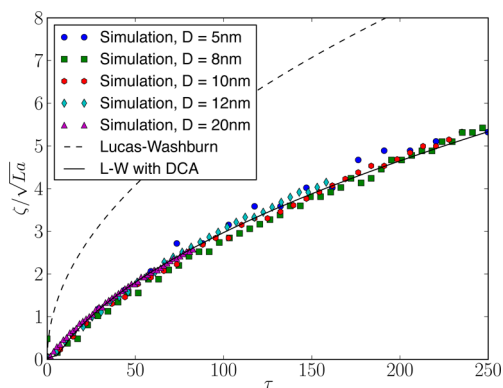


Figure 4. Imbibition length in reduced units, normalized by the square root of the Laplace number as a function of the time in reduced units. The data from simulations of all nanopore diameters collapse onto a single curve that can be well described by the modified Lucas–Washburn equation that accounts for the DCA (eq 10 with $C_d = 0.37$). The classical Lucas–Washburn equation, also with $C_d = 0.37$, is shown for comparison.

effect, equivalent to using a correction factor for Poiseuille flow assumption, as is often done in modeling small-scale channels.

The initial similarity in imbibition rate seen in Figure 2 is unexpected according to the classical Lucas–Washburn theory, which predicts a $\sqrt{R_v}$ scaling for the imbibition length as a function of time. This discrepancy can be explained by looking at the dependence of I on radius. To compute I , the DCA must be known. To obtain θ_D as a function of time, we extracted the value directly from the imbibition simulations and computed the numerical integral, I , at time t using cubic interpolation between data points. Figure 3a shows $R_v I$ plotted as a function of time, which according to the theoretical description must be directly related to the imbibition length. The curves overlap for the first 2 ns and then diverge systematically. This finding supports the earlier observation that as $t \rightarrow 0$, the scaling of I with radius asymptotes to $1/R_v$ (Figure 3b), canceling out the radius dependence in the prefactor to the integral in eq 9. This analysis explains why the imbibition rates at the early stages of the simulations show nanopore size-independence. Theoretical models for dynamic contact angles^{32–34} predict a scaling with capillary number, $Ca = (\eta V)/\gamma$, and local dissipation mechanisms at the three-phase contact line, but this dependence cannot explain the differences observed in these simulations. Over the initial few nanoseconds, the imbibition rates and hence Ca are approximately the same for all nanopore sizes, yet the contact angles clearly display a dependence on the nanopore radius (Figure 5a, inset). Thus, a size effect independent of Ca must contribute to the DCA. The size effect present in the DCA is even clearer in Figure 5b, where the cube of the contact angle is plotted as a function of Ca . Additionally, the data for θ_D^3 appear roughly linear when plotted as a function of Ca , suggesting the scaling predicted by theoretical considerations³³ still holds, separate from the size effect. The observation of a size effect appears to be in line with experimental and theoretical results that suggest that the DCA is not simply a function of the capillary number, but instead depends nonlocally on the entire flow field.^{35–37} According to ref 36, the DCA results from the starvation of density at the contact line relative to the equilibrium density at the liquid–solid interface. This is related to competition between the velocity into the contact line along the free surface and the velocity at which the solid–liquid interface drags fluid away

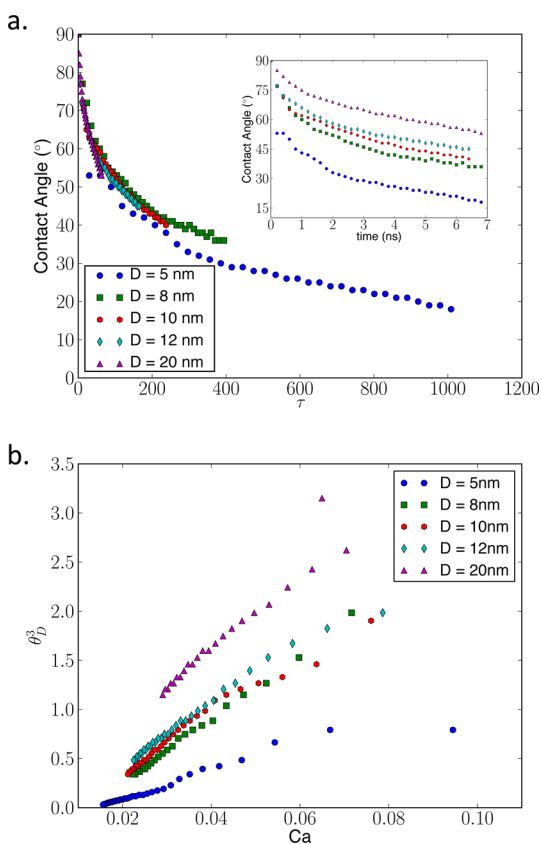


Figure 5. (a) Dynamic contact angle as a function of time in reduced units. At $\tau = 0$, all simulations have a contact angle of 90° . The data nearly collapse, suggesting the dynamic contact angle evolves according to a characteristic time-scale that is proportional to R_v^2 . Inset shows the strong dependence of dynamic contact angle on nanopore diameter when no time normalization is performed. (b) Cube of dynamic contact angle as a function of capillary number. If no size dependence was present, all data should overlap, clearly showing a size effect on the dynamic contact angle that is independent of meniscus velocity.

from the contact line. In the curtain coating process studied in ref 36, the substrate velocity is a well-defined input parameter that is independent of contact angle. However, the imbibition process studied here is more complicated in that the imbibition velocity (substrate velocity) is intimately coupled to the contact angle, which, in turn, is a function of the relative velocity of the free surface with respect to imbibition velocity. Characterization of the interplay between the velocity field and contact angle is currently the subject of ongoing research.

To further characterize the DCA's dependence on nanopore radius, the modified Lucas–Washburn equation can be written conveniently in a nondimensionalized form using a nondimensional length scale $\zeta = z/R_v$, and a nondimensional time scale $\tau = t/t_v$. It may seem odd to normalize time by the viscous time scale even though viscous effects are relatively unimportant. However, normalizing by t_v effectively scales the time by the radius squared, which turns out to be a convenient scaling (see below). Solving eq 8 for ζ , we arrive at

$$\zeta(\tau) = \sqrt{2C_d La \int \cos(\theta_D(\tau)) d\tau} \quad (10)$$

where the Laplace number is defined as $La = (\gamma\rho R_v)/(\eta^2)$.

Interestingly, plotting $(\zeta)/(La)^{1/2}$ as a function of τ collapses all of the simulation data onto a single curve (Figure 4). This implies that the only channel radius dependence in eq 10 is contained in the Laplace number, and hence the dynamic contact angle as a function of τ is a roughly identical across simulations. Plotting $\theta_D(\tau)$ as a function of τ (Figure 5) shows precisely this: the dynamic contact angle for channels of different radii collapses onto a single curve when plotted against the normalized time scale. From the inset in Figure 5, it is clear that the contact angles approach the equilibrium values much more rapidly for small channels. However, for all cases, the decaying of the dynamic contact angle in time is of a similar form and can be characterized by a time scale proportional to the square of the radius, or equivalently the cross-sectional area of the nanopore.

This collapse suggests a similarity between imbibition into different size capillaries at the nanoscale that could be useful for nanofluidics experiments. By carrying out experiments with a single channel diameter and analyzing data in ζ – τ space, one can predict the key material parameters empirically and eliminate the need for manufacturing a range of different size capillaries, which can be a time-consuming and costly process. Furthermore, the scaling concepts presented here hold for a broad range of nanopore diameters (5–20 nm) that are relevant to the size range of nanopores that can currently be fabricated and characterized. Experimental characterization of the size-scaling of hydrophilic nanopores has not yet been carried out; however, we envision that the predictions made by our model can guide and be validated by systematic nanofluidics experiments in the near future.

CONCLUSION

In this work, we have presented a calibrated a coarse-grained water model coupled with a DPD thermostat that is capable of modeling nanofluidic systems in confined geometries while retaining the particle nature of the fluid. Utilizing the capabilities of this model, we investigated imbibition of water into nanoscopic pores at length and time scales that exceed all-atom MD simulations. The dramatic speed-up gained by the computational model allowed us to carry out the first systematic simulation study on the dependence of imbibition dynamics as a function of nanopore diameter. In particular, we characterized the size effect on the dynamic contact angle in terms of a dimensionless time scale and found that a size effect exists that cannot be explained through typical relations between the contact angle and capillary number. We speculate that this could be the result of nonlocal influences of the flow field on the contact angle, but further investigation is required to verify this suggestion. Additionally, we have shown that a nondimensionalized form of the Lucas–Washburn equation that accounts for the DCA size effect is capable of capturing the behavior of water over the range of nanopore diameters simulated. The generality of this equation with respect to nanopore dimension could be useful in comparing experiments of different sizes or extrapolating results to dimensions that are difficult to investigate experimentally.

Looking forward, the adaptability of the model opens the door for a range of further applications. For instance, this model could be useful for investigating a range of wetting phenomena such as the influence of hierarchical surface topology on the dynamics of drops in contact with superhydrophobic surfaces. Additionally, this model could easily be extended to model two-phased flows such as polymer melts

with high water content, or macromolecular transport through nanochannels.

■ ASSOCIATED CONTENT

■ Supporting Information

Viscosity calibration results, and equilibrium contact angle calculations. This material is available free of charge via the Internet at <http://pubs.acs.org>.

■ AUTHOR INFORMATION

Corresponding Author

*E-mail: s-keten@northwestern.edu (S.K.); w-liu@northwestern.edu (W.K.L.).

Notes

The authors declare no competing financial interest.

[†]Distinguished World Class University Professor, Sung Kyun Kwan University, Korea.

■ ACKNOWLEDGMENTS

W.S. and W.K.L. were supported by NSF CMMI Grants 0856492 and 0856333. S.K. acknowledges support from the Civil and Environmental Engineering and Mechanical Engineering Departments at Northwestern University. We acknowledge a supercomputing grant from Quest High Performance Computing Center at Northwestern University. W.K.L. was partially supported by the World Class University Program through the National Research Foundation of Korea (NRF) funded by the Ministry of Education, Science and Technology (R33-10079).

■ ABBREVIATIONS

CGMD, coarse-grained molecular dynamics; MD, molecular dynamics; DPD, dissipative particle dynamics; LJ, Lennard–Jones; DCA, dynamic contact angle; LW, Lucas–Washburn

■ REFERENCES

- (1) Hummer, G.; Rasaiah, J. C.; Noworyta, J. P. Water conduction through the hydrophobic channel of a carbon nanotube. *Nature* **2001**, *414*, 188–190.
- (2) Pascal, T. A.; Goddard, W. A.; Jung, Y. Entropy and the driving force for the filling of carbon nanotubes with water. *Proc. Natl. Acad. Sci. U.S.A.* **2011**, *108*, 11794–11798.
- (3) Ananta, J. S.; Godin, B.; Sethi, R.; Moriggi, L.; Liu, X. W.; Serda, R. E.; Krishnamurthy, R.; Muthupillai, R.; Bolskar, R. D.; Helm, L.; Ferrari, M.; Wilson, L. J.; Decuzzi, P. Geometrical confinement of gadolinium-based contrast agents in nanoporous particles enhances T(1) contrast. *Nat. Nanotechnol.* **2010**, *5*, 815–821.
- (4) Persson, B. N. J. Capillary adhesion between elastic solids with randomly rough surfaces. *J. Phys.: Condens. Matter* **2008**, *20*, ???.
- (5) Nealey, P. F.; Yoshimoto, K.; Stoykovich, M. P.; Cao, H. B.; de Pablo, J. J.; Dragan, W. J. A two-dimensional model of the deformation of photoresist structures using elastoplastic polymer properties. *J. Appl. Phys.* **2004**, *96*, 1857–1865.
- (6) Aizenberg, J.; Kang, S. H.; Pokroy, B.; Mahadevan, L. Control of shape and size of nanopillar assembly by adhesion-mediated elastocapillary interaction. *ACS Nano* **2010**, *4*, 6323–6331.
- (7) Priezjev, N. V.; Troian, S. M. Influence of periodic wall roughness on the slip behaviour at liquid/solid interfaces: molecular-scale simulations versus continuum predictions. *J. Fluid Mech.* **2006**, *554*, 25–46.
- (8) Yesylevskyy, S. O.; Schafer, L. V.; Sengupta, D.; Marrink, S. J. Polarizable water model for the coarse-grained MARTINI force field. *PLoS Comput. Biol.* **2010**, *6*, e1000810.

(9) Chiu, S. W.; Scott, H. L.; Jakobsson, E. A coarse-grained model based on Morse potential for water and n-alkanes. *J. Chem. Theory Comput.* **2010**, *6*, 851–863.

(10) Soddemann, T.; Dunweg, B.; Kremer, K. Dissipative particle dynamics: A useful thermostat for equilibrium and nonequilibrium molecular dynamics simulations. *Phys. Rev. E* **2003**, *68*, 046702.

(11) Groot, R. D.; Warren, P. B. Dissipative particle dynamics: Bridging the gap between atomistic and mesoscopic simulation. *J. Chem. Phys.* **1997**, *107*, 4423–4435.

(12) Patrick B, W. Dissipative particle dynamics. *Curr. Opin. Colloid Interface Sci.* **1998**, *3*, 620–624.

(13) Hoogerbrugge, P. J.; Koelman, J. M. V. A. Simulating microscopic hydrodynamic phenomena with dissipative particle dynamics. *Europhys. Lett.* **1992**, *19*, 155–160.

(14) Espanol, P.; Warren, P. Statistical-mechanics of dissipative particle dynamics. *Europhys. Lett.* **1995**, *30*, 191–196.

(15) Pagonabarraga, I.; Frenkel, D. Dissipative particle dynamics for interacting systems. *J. Chem. Phys.* **2001**, *115*, 5015–5026.

(16) Warren, P. B. Vapor-liquid coexistence in many-body dissipative particle dynamics. *Phys. Rev. E* **2003**, *68*, 066702.

(17) Dimitrov, D. I.; Milchev, A.; Binder, K. Capillary rise in nanopores: Molecular dynamics evidence for the Lucas–Washburn equation. *Phys. Rev. Lett.* **2007**, *99*, 054501.

(18) Ahadian, S.; Mizuseki, H.; Kawazoe, Y. On the kinetics of the capillary imbibition of a simple fluid through a designed nanochannel using the molecular dynamics simulation approach. *J. Colloid Interface Sci.* **2010**, *352*, 566–572.

(19) Marrink, S. J.; Risselada, H. J.; Yefimov, S.; Tieleman, D. P.; de Vries, A. H. The MARTINI force field: Coarse grained model for biomolecular simulations. *J. Phys. Chem. B* **2007**, *111*, 7812–7824.

(20) Chen, C.; Gao, C.; Zhuang, L.; Li, X.; Wu, P.; Dong, J.; Lu, J. A many-body dissipative particle dynamics study of spontaneous capillary imbibition and drainage. *Langmuir* **2010**, *26*, 9533–9538.

(21) Cupelli, C.; Henrich, B.; Glatzel, T.; Zengerle, R.; Moseler, M.; Santer, M. Dynamic capillary wetting studied with dissipative particle dynamics. *New J. Phys.* **2008**, *10*.

(22) Martic, G.; Gentner, F.; Seveno, D.; Coulon, D.; De Coninck, J.; Blake, T. D. A molecular dynamics simulation of capillary imbibition. *Langmuir* **2002**, *18*, 7971–7976.

(23) Plimpton, S. Fast parallel algorithms for short-range molecular dynamics. *J. Comput. Phys.* **1995**, *117*, 1–19.

(24) Humphrey, W.; Dalke, A.; Schulten, K. VMD: Visual molecular dynamics. *J. Mol. Graphics* **1996**, *14*, 33.

(25) Marsh, C. A.; Backx, G.; Ernst, M. H. Static and dynamic properties of dissipative particle dynamics. *Phys. Rev. E* **1997**, *56*, 1676–1691.

(26) Noguchi, H.; Gompper, G. Transport coefficients of off-lattice mesoscale-hydrodynamics simulation techniques. *Phys. Rev. E* **2008**, *78*, e016706.

(27) Allen, M. P.; Tildesley, D. J. *Computer Simulation of Liquids*; Clarendon Press: Oxford, 1989.

(28) Washburn, E. W. The dynamics of capillary flow. *Phys. Rev.* **1921**, *17*, 273–283.

(29) Lucas, R. Ueber das zeitgesetz des kapillaren aufstiegs von flüssigkeiten. *Kolloid Z.* **1918**, *23*, 15.

(30) Stukan, M. R.; Ligneul, P.; Crawshaw, J. P.; Boek, E. S. Spontaneous imbibition in nanopores of different roughness and wettability. *Langmuir* **2010**, *26*, 13342–13352.

(31) Bosanquet, C. H. On the flow of liquids into capillary tubes. *Philos. Mag.* **1923**, *45*, 525–531.

(32) de Gennes, P. G. a. B.-W., F.; Quere, D. *Capillarity and Wetting Phenomena: Drops, Bubbles, Pearls, Waves*; Springer: New York, 2003.

(33) Eggers, J.; Stone, H. A. Characteristic lengths at moving contact lines for a perfectly wetting fluid: the influence of speed on the dynamic contact angle. *J. Fluid Mech.* **2004**, *505*, 309–321.

(34) Brochardwyart, F.; Degennes, P. G. Dynamics of partial wetting. *Adv. Colloid Interface Sci.* **1992**, *39*, 1–11.

(35) Blake, T. D.; Bracke, M.; Shikhmurzaev, Y. D. Experimental evidence of nonlocal hydrodynamic influence on the dynamic contact angle. *Phys. Fluids* **1999**, *11*, 1995–2007.

(36) Lukyanov, A. V.; Shikhmurzaev, Y. D. Effect of flow field and geometry on the dynamic contact angle. *Phys. Rev. E* **2007**, *75*, 051604.

(37) Clarke, A.; Stattersfield, E. Direct evidence supporting nonlocal hydrodynamic influence on the dynamic contact angle. *Phys. Fluids* **2006**, *18*, 048106.